Occupancy-MAE: Self-supervised Pre-training Large-scale LiDAR Point Clouds with Masked Occupancy Autoencoders

Chen Min[1,*] and Dawei Zhao[2] and Jiaolong Xu[2]
and Liang Xiao[2] and Yiming Nie[2] and Bin Dai[2]
[1]Peking University
[2]NIIDT

minchen@stu.pku.edu.cn

Abstract

Current perception models in autonomous driving rely heavily on large-scale labeled LiDAR data, which is costly and time-consuming to annotate. In this work, we aim to facilitate research on self-supervised masked learning using the vast amount of unlabeled LiDAR data available in autonomous driving. However, existing masked point autoencoding methods only focus on small-scale indoor point clouds and struggle to adapt to outdoor scenes, which usually have a large number of non-evenly distributed LiDAR points. To address these challenges, we propose a new self-supervised masked learning method named Occupancy-MAE, specifically designed for large-scale outdoor LiDAR points. We leverage the gradually sparse occupancy structure of large-scale outdoor LiDAR point clouds and introduce a range-aware random masking strategy and a pretext task of occupancy prediction. Occupancy-MAE randomly masks voxels of LiDAR point clouds based on their distance to LiDAR and predicts the masked occupancy structure of the whole 3D scene. This simple occupancy prediction objective encourages Occupancy-MAE to extract high-level semantic information to recover the masked voxel from only a small amount of visible voxels. Extensive experiments demonstrate the effectiveness of Occupancy-MAE across several downstream tasks. For the 3D object detection task, Occupancy-MAE reduces the labeled data required for car detection on KITTI by half and boosts small object detection by around 2% mAP on Waymo. For the 3D semantic segmentation task, Occupancy-MAE outperforms training from scratch by around 2% mIOU on nuScenes. For the unsupervised domain adaptation task, Occupancy-MAE improves the performance by about 0.5% ∼ 1% mAP. Our results show that it is feasible to pre-train unlabeled large-scale LiDAR point clouds with masked autoencoding to enhance the 3D perception ability of autonomous driving.
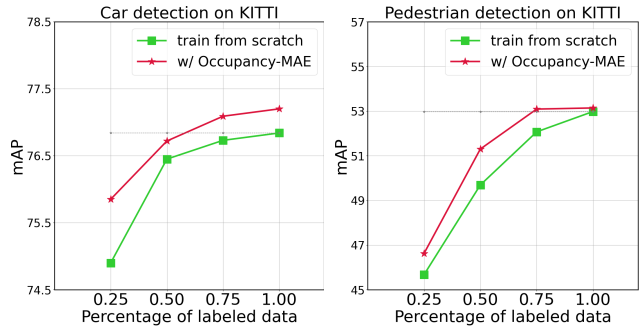
Figure 1. **Label-efficiency of our self-supervised pre-training**. Occupancy-MAE outperforms training from scratch and achieves the same detection performance with fewer labeled data (about 50% for the car class and 75% for the pedestrian class).

1. Introduction

Accurate 3D perception is a core technique in autonomous driving, as it enables vehicles to obtain precise information about their surroundings. Numerous large-scale outdoor LiDAR point cloud datasets such as KITTI [13], Waymo [30], nuScenes [1], and ONCE [25] have been published, showcasing the potential of environmental perception for unmanned vehicles. However, the collection and annotation of large-scale LiDAR point clouds for common tasks like 3D object detection and semantic segmentation can be extremely time-consuming and labor-intensive. For instance, skilled workers can only annotate around 100-200 frames per day [25]. Therefore, self-supervised learning using large-scale unannotated LiDAR point clouds is crucial for enhancing the perceptual ability of autonomous driving. It may pave the way for developing the next-generation, industry-level autonomous driving perception model that is both powerful and robust [25].

Self-supervised learning has made significant strides in recent years, enabling pre-training of rich features without human annotations. The simple masked autoencoding ap-
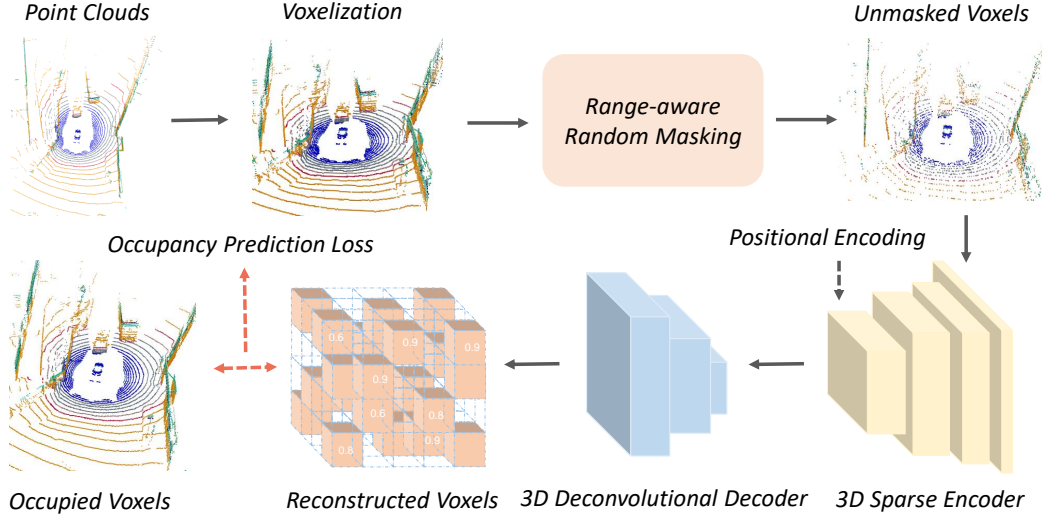
1

Figure 2. The overall architecture of our Occupancy-MAE. We first transform the large-scale irregular LiDAR point clouds into volumetric representations, randomly mask the voxels according to their distance from the LiDAR sensor (i.e., range-aware masking strategy), then reconstruct the occupancy values of voxels with an asymmetric autoencoder network. We adopt the 3D Spatially Sparse Convolutions [39] with positional encoding as the encoding backbone. We apply binary occupancy classification as the pretext task to distinguish whether the voxel contains points. After pre-training, the lightweight decoder is discarded, and the encoder is used to warm up the backbones of downstream tasks.

proach has been particularly effective in learning representative features, where the task is to reconstruct masked data from unmasked input [9, 18, 6, 36]. In natural language processing, masked autoencoding has enabled the training of large language models, such as ChatGPT [33]. Similarly, in 2D vision, masked autoencoding has outperformed supervised pre-training counterparts [18].

Recently, several works on masked point autoencoding have been proposed, such as Point-MAE [26], Point-BERT [42], MaskPoint [23], and Point-M2AE [43]. However, these methods have primarily focused on small-scale point clouds, such as synthetic point cloud datasets like ShapeNet [5] and indoor point cloud datasets like Scan-Net [7]. In contrast, masked autoencoding for large-scale outdoor LiDAR point clouds [13, 30, 1, 25], has received less attention. Training from scratch on large-scale labeled LiDAR point clouds remains the dominant approach [25]. To introduce the idea of masked autoencoding to self-supervised learning on large-scale outdoor LiDAR point clouds, we first identify the challenges compared to masked small-scale point cloud autoencoding works [42, 26, 23, 43], and then propose solutions:

Firstly, small-scale point clouds [5, 7] differ from large-scale outdoor LiDAR point clouds [13, 30, 1, 25] in several ways. (1) Small-scale point clouds typically contain far fewer points than their large-scale counterparts, with ShapeNet containing approximately 2k points and ScanNet downsampled to about 2k points for use in masked small-scale point cloud autoencoding works [42, 26, 23, 43]. In

contrast, LiDAR sensors such as the Velodyne HDL-64E LiDAR can scan up to 192,000 points per frame, covering an area of $160 \times 160 \times 20$ meters [37]. (2) Small-scale point clouds are often evenly distributed, while large-scale LiDAR point clouds become sparser as distance from the LiDAR sensor increases. (3) Existing masked small-scale point cloud autoencoding works [42, 26, 23, 43] typically rely on furthest point sampling (FPS) and k-nearest neighbors (kNN) to divide points into equal subsets, which is not suitable for large-scale outdoor LiDAR point clouds. The challenge of processing such large-scale point clouds efficiently, and in real-time, has been highlighted in previous works [46, 37], making pre-training on these datasets a more challenging task.

Secondly, existing masked small-scale point clouds autoencoding works [42, 26, 43] mainly focus on regressing the missing points. However, it is not appropriate to reconstruct the features of large-scale LiDAR point clouds through regression, as these features contain essential spatial information [39]. Moreover, the positional encoding of voxels can offer a shortcut for the decoder [35]. To address this issue, we shift our focus to the occupancy distribution of large-scale LiDAR point clouds and design the occupancy prediction objective as the pretext task. By doing so, the network is forced to learn representative features to recover the overall structure of the 3D scene, making this simple task an effective solution for our pre-training method.

Thirdly, the random masking strategy used in existing masked small-scale point clouds autoencoding works [42,

26, 23, 43] may not be suitable for large-scale outdoor LiDAR point clouds due to their uneven distribution. Unlike small-scale point clouds, the density of large-scale LiDAR point clouds varies based on the distance to LiDAR sensor. Hence, a uniform random masking strategy for all voxels would not be optimal. We propose a range-aware random masking strategy for large-scale LiDAR point clouds to address this. This strategy adjusts the masking ratio based on the voxel's distance to the LiDAR sensor, with the masking ratio decreasing as the distance from the sensor increases.

Fourthly, while the Transformer with self-attention mechanism works well for small-scale point clouds [42, 26, 23, 43], it becomes computationally expensive and impractical for larger point clouds with hundreds of thousands of unmasked 3D voxels. As a solution, some methods [11, 17, 20] have used pillar-based representation to apply Transformer. However, this approach could lose valuable information in the vertical axis. To address this, the paper proposes to use 3D Sparse Convolutions [39] with a positional encoding module in the encoder. This allows the network to focus on visible 3D voxels instead of processing the entire point cloud, significantly reducing the computational cost. The positional encoding module, similar to the positional embeddings used in Transformers, encodes the spatial information of the voxels into a fixed-size embedding vector. This approach effectively captures the positional information of the voxels and enables the network to learn spatially-aware features.

Occupancy prediction is a commonly used approach in environment representation for autonomous driving tasks. It involves dividing the environment into a grid and estimating the probability of each cell being occupied or free. This approach has been applied in various tasks such as obstacle detection, path planning, and simultaneous localization and mapping (SLAM) [12, 24, 21]. Recently, Tesla proposed a vision-based occupancy network approach for autonomous driving, allowing the car to perceive and navigate through space by determining whether or not it is safe to drive in that space [8]. For LiDAR point clouds, occupancy can be defined as whether or not a voxel in the 3D grid contains points. LiDAR point clouds are information-redundant, making them suitable for masked autoencoding methods to learn rich and representative features.

Driven by the above analyses, we propose a novel self-supervised learning framework, called **Occupancy-MAE**, for pre-training large-scale outdoor LiDAR point clouds using masked occupancy autoencoding. Figure 2 illustrates the workflow of our Occupancy-MAE, which first employs the range-aware masking strategy to mask voxels randomly, and then feeds the unmasked voxels into the 3D sparse encoder. The output of the 3D decoder is the probability that each voxel contains points, and we calculate the binary occupancy classification loss to pre-train the network. Train-

ing on the pretext task of masked occupancy classification encourages the encoder network to be voxel-aware of the entire object shape, thereby learning representative features for 3D perception.

After analyzing the results of our experiments, we conclude that Occupancy-MAE is a simple and effective self-supervised learning framework that can generalize well across various downstream tasks. In the 3D object detection task, our method outperforms the state-of-the-art self-supervised learning methods by $0.5\% \sim 6\%$ mAP on ONCE dataset, which is a recently published dataset for self-supervised learning on large-scale LiDAR point clouds. Moreover, pre-training with Occupancy-MAE can significantly improve the performance of popular 3D detectors such as SECOND [39], PV-RCNN [27], CenterPoint [41], and PV-RCNN++ [28] trained from scratch on KITTI, Waymo, and nuScenes datasets, especially for small objects. As illustrated in Figure 1, Occupancy-MAE is a data-efficient learner that can effectively train large-scale LiDAR point clouds with limited annotated 3D data. For the 3D semantic segmentation task, Occupancy-MAE with a two-layer decoder can improve the training from scratch by about 2% mIOU. We also demonstrate the effectiveness of our approach in the unsupervised domain adaptation task, which confirms the transfer learning ability of Occupancy-MAE. Even with a 90% masking ratio, Occupancy-MAE can still learn representative features as large-scale LiDAR point clouds are information redundant, which ultimately improves the performance of 3D perception.

The main contributions of this work are listed below:

- We present a data-efficient learning framework called Occupancy-MAE, which uses masked autoencoding to pre-train large-scale outdoor LiDAR point clouds, reducing the need for expensively annotated data.

- We propose an occupancy prediction pretext task that leverages the gradually sparse occupancy structure of large-scale LiDAR point clouds. By recovering the masked occupancy distribution of the 3D scene from a small number of visible voxels, the network is forced to extract high-level semantic information.

- We introduce the range-aware random masking strategy to take advantage of the varying density of large-scale LiDAR point clouds, which improves the pre-training performance.

- Our proposed Occupancy-MAE significantly outperforms training from scratch on various downstream tasks, including 3D object detection, semantic segmentation, and unsupervised domain adaptation.

2. Related Work

2.1. Self-supervised Learning

Self-supervised Learning (SSL) has gained popularity in recent years as an effective approach to avoiding costly data annotation. The pretext task of predicting the relative location of image patches was proposed in [10]. Methods in [14, 38, 34] have designed rotation prediction tasks, which have shown promising results in learning representative features. In [2], a jigsaw puzzle prediction task is introduced, which generalizes well in domain adaptation for object recognition. DeepCluster [3] and SwAV [4] obtain pseudo labels with k-means clustering and use these labels to train networks. Other methods such as Moco [19], Point-Contrast [35], BYOL [16], and DepthConstrast [44] construct contrastive views for self-supervised learning. Recently, MAE [18] has shown promising results in self-supervised learning by first masking random patches of the input image and then reconstructing the missing pixels with a simple autoencoder framework. VideoMAE [32] extends the MAE into spatiotemporal representation learning from videos, which have greater information redundancy. Our Occupancy-MAE follows the design philosophy of MAE and applies it to large-scale outdoor LiDAR point clouds based on their geometric characteristics, such as sparsity and varying density.

2.2. Masked autoencoders for point clouds

Masked autoencoding has achieved success in NLP [9] and image [18], leading to the development of masked autoencoding techniques for point clouds in the last year. Point-BERT [42] first introduces MAE to pre-train small-scale point clouds. Point-MAE [26] reconstructs the small-scale point patches with the Chamfer distance. Mask-Point [23] designs the decoder for discriminating the small-scale masked point patches. Point-M2AE [43] applies the pyramid architectures to model spatial geometries and capture both fine-grained and high-level semantics of 3D shapes. However, these methods focusing on small-scale indoor point clouds cannot process large-scale outdoor LiDAR point clouds under the property of a large range of scenes and varying density. Voxel-MAE [20] adopts masked autoencoding for large-scale point clouds, but is limited to only pillar-based methods, which will lose vertical information. Our proposed Occupancy-MAE overcomes these limitations and enables pre-training of large-scale LiDAR point clouds for both voxel and pillar-based methods.

3. Methodology

Given the instances from large-scale LiDAR point clouds, self-supervised pre-training is to train the network with the unlabeled data to generate representative features.

Inspired by the excellent performance of masked autoencoding [9, 18, 26], we design the masked voxel autoencoding network for 3D perception. The proposed Occupancy-MAE randomly masks the voxels and then reconstructs the occupancy values of voxels with an autoencoder network. The pretext task of occupancy prediction is trained with the cross-entropy loss.

With the n_s unlabeled point cloud data $\left\{ \mathbf{X}^i \right\}_{i=1}^{n_s}$, we aim to first pre-train the masked autoencoding network ϕ_{pre} to learn the high-level semantics. Then we use the pre-trained model to warm up the network ϕ_s of downstream tasks. We also extend the pre-training method to domain adaptive task on the target point clouds $\left\{ \mathbf{X}^j \right\}_{j=1}^{n_t}$.

3.1. Range-aware Random Masking

In this work, we adopt the common approach of dividing the point clouds into spaced voxels, which is often used in 3D perception models [39, 46]. For a point cloud with dimensions $W \times H \times D$ along the $X \times Y \times Z$ axes, the size of each voxel is $v_W \times v_H \times v_D$, resulting in a total of n_l voxels, of which n_v contain points. Voxel-based methods are more computationally efficient than point-based methods [29], making them well-suited for processing large-scale LiDAR point clouds in applications such as self-driving cars.

While the masking strategy has been proven effective in pre-training models for language, images, and small-scale point clouds, the distribution of large-scale LiDAR point clouds is unique due to their sparsity levels being correlated with distance from the LiDAR sensor. Points close to sensor are densely packed, while those further away are much more sparse. Therefore, we cannot apply the same masking strategy to both near-range and far-range points. Instead, we propose a range-aware random masking strategy that masks a small percentage of data for far-range points.

To this end, we introduce the range-aware random masking strategy which takes into account the distance information. This strategy divides the occupied voxels into three groups based on their distance from the LiDAR sensor: 0-30 meters, 30-50 meters, and >50 meters. The masking ratio decreases as the distance increases, and we use a piecewise approach to apply the random masking strategy to each group. The corresponding numbers of voxels are n_{v1}, n_{v2}, and n_{v3}. It is noted that more division groups are also applicable but will cause lots of preprocessing time in pre-training. We take the random masking strategy for each group with the descending masking ratio $r1$, $r2$, and $r3$ (i.e., $r1 > r2 > r3$). Thus the number of unmasked occupied voxels is $n_{un} = n_{v1}(1 - r1) + n_{v2}(1 - r2) + n_{v3}(1 - r3)$, and the set of voxels $\mathbf{V}_{input} \in R^{n_{un} \times 4}$ is used as training data. The occupied voxels containing points (the value of each voxel is 1) and the empty voxels (the value of each voxel is 0) are used as ground truth $\mathbf{T} \in R^{n_l \times 1}$ for occupancy classification loss.

Method	Vehicle				Pedestrian				Cyclist				mAP
	overall	0-30m	30-50m	50m-inf	overall	0-30m	30-50m	50m-inf	overall	0-30m	30-50m	50m-inf	
SECOND [39]	71.19	84.04	63.02	47.25	26.44	29.33	24.05	18.05	58.04	69.96	52.43	34.61	51.89
BYOL [16]	68.02	81.01	60.21	44.17	19.50	22.16	16.68	12.06	50.61	62.46	44.29	28.18	46.04
DepthContrast [44]	71.88	84.26	65.58	49.97	23.57	26.36	21.15	14.39	56.63	68.26	50.82	34.67	50.69
SwAV [4]	72.71	83.68	65.91	50.10	25.13	27.77	22.77	16.36	58.05	69.99	52.23	34.86	51.96
DeepCluster [3]	73.19	84.25	66.86	50.47	24.00	26.36	21.73	16.79	58.99	70.80	53.66	36.17	52.06
Point-MAE [26]	71.78	84.07	65.52	50.97	23.07	25.95	21.09	15.26	56.87	68.79	51.54	32.49	50.57
MaskPoint [23]	71.63	83.79	65.65	50.39	24.67	27.21	22.64	15.98	57.08	69.07	51.95	32.84	51.13
Occupancy-MAE	72.78	83.77	66.01	50.26	27.49	30.54	25.28	16.11	57.26	69.71	52.31	33.51	**52.51**

Table 1. Quantitative detection performance achieved by different self-supervised learning methods on the ONCE *val* set. The pre-training process is on the unlabeled small set that contains 100k scenes.

Method	Car		Cyclist	
	3D	BEV	3D	BEV
SECOND [39]	72.55	83.77	52.08	56.05
Occupancy-MAE + SECOND	**72.87**	**83.96**	**54.84**	**60.67**

Table 2. Performance comparison on the KITTI test split evaluated by the mean Average Precision with 40 recall positions at a moderate difficulty level.

Method	Car	Pedestrian	Cyclist
PointPillars [22]	77.28	52.29	62.68
Voxel-MAE [20] + PointPillars	77.33	52.42	63.12
Occupancy-MAE + PointPillars	**77.48**	**53.35**	**64.73**

Table 3. Performance comparison on the KITTI *val* split evaluated by the mean Average Precision with 11 recall positions at moderate difficulty level.

3.2. 3D Sparse Convolutional Encoder

The Transformer network used in masked autoencoding for NLP [9], 2D vision [18], and small-scale point clouds [26, 23] performs self-attention on unmasked portions of the training data, which are unaffected by the masking. However, with millions of points in a 3D scene, even after masking 90% of voxels, there are still hundreds of thousands of unmasked voxels, making it impractical for the Transformer network to aggregate information from such a vast amount of input data [9]. To address this, the 3D Sparse Convolution [15, 39] was proposed for processing large-scale point clouds. This approach uses positional encoding to aggregate information only from occupied voxels, resulting in high efficiency. Popular 3D perception methods [39, 27, 41, 46] have since been developed using this technique. Motivated by this, we adopt the 3D Spatially Sparse Convolution from SECOND [39] to build our encoder network, allowing us to aggregate information only from unmasked, occupied voxels using the positional encoding module. Our voxel masking strategy thus reduces the memory complexity of training, similar to how the Transformer network works in NLP [9], 2D vision [18], and small-scale point clouds [26, 23, 42, 43].

3.3. 3D Deconvolutional Decoder

Our decoder is composed of 3D Deconvolutional layers, with the last layer outputting the probability of each voxel containing points, resulting in an output tensor $\mathbf{P} \in R^{n_l \times 1}$. During pre-training, the decoder's only purpose is to perform occupied voxel reconstruction. By shifting the masked tokens to the decoder, we encourage the encoder to learn better latent features for downstream tasks. The decoder is lightweight, consisting of only two or three 3D Deconvolutional layers, making it scalable to larger perception ranges.

3.4. Reconstructed Occupancy Target

The main objective of most masked autoencoding works is to reconstruct the masked parts through a regression task [26, 42, 43], which is not challenging for the network due to the positional encoding of voxels. However, in 3D perception, the occupancy structure of the 3D scene plays a crucial role in perception models [45, 39, 46]. For instance, Tesla introduced the Occupancy Networks for autonomous driving [8] last year. Motivated by this, we propose the occupancy prediction task for large-scale outdoor LiDAR point clouds pre-training, aiming to encourage the network to reason over high-level semantics to recover the masked occupancy distribution of the 3D scene from a small number of visible voxels. To accomplish this, we calculate the binary occupancy classification loss of cross-entropy using the predicted occupied voxels $\mathbf{P}$ and the ground truth occupied voxels $\mathbf{T}$.

$$loss = -\frac{1}{batch} \sum_{i=1}^{batch} \sum_{j=1}^{n_l} \mathbf{T}_j^i log \mathbf{P}_j^i, \qquad (1)$$

where $\mathbf{P}_j^i$ is the predicted probability of voxel j of the i-th training sample, and $\mathbf{T}_j^i$ is the corresponding ground truth whether the voxel contains point clouds.

Method	Vec_L1		Vec_L2		Ped_L1		Ped_L2		Cyc_L1		Cyc_L2	
	mAP	mAPH	mAP	mAPH	mAP	mAPH	mAP	mAPH	mAP	mAPH	mAP	mAPH
CenterPoint [41]	71.33	70.76	63.16	62.65	72.09	65.49	64.27	58.23	68.68	67.39	66.11	64.87
Occupancy-MAE + CenterPoint	**71.89**	**71.33**	**64.05**	**63.53**	**73.85**	**67.12**	**65.78**	**59.62**	**70.29**	**69.03**	**67.76**	**66.53**
PV-RCNN [27]	75.41	74.74	67.44	66.80	71.98	61.24	63.70	53.95	65.88	64.25	63.39	61.82
Occupancy-MAE + PV-RCNN	**75.94**	**75.28**	**67.94**	**67.34**	**74.02**	**63.48**	**64.91**	**55.57**	**67.21**	**65.49**	**64.62**	**63.02**
PV-RCNN++ [28]	77.82	77.32	69.07	68.62	77.99	71.36	69.92	63.74	71.80	70.71	69.31	68.26
Occupancy-MAE + PV-RCNN++	**78.25**	**77.67**	**69.56**	**69.32**	**79.85**	**73.24**	**71.15**	**64.99**	**71.85**	**70.75**	**69.37**	**68.33**

Table 4. Quantitative detection performance on the Waymo *val* set. The models are trained on 20% Waymo training set.

Method	mAP	NDS	mATE	mASE	mAOE	mAVE	mAAE
SECOND [39]	50.59	62.29	31.15	25.51	26.64	26.26	20.46
Occupancy-MAE + SECOND	**50.82**	**62.45**	**31.02**	**25.23**	**26.12**	**26.11**	**20.04**
CenterPoint [41]	56.03	64.54	30.11	25.55	**38.28**	21.94	18.87
Occupancy-MAE + CenterPoint	**56.45**	**65.02**	**29.73**	**25.17**	38.38	**21.47**	**18.65**

Table 5. Quantitative detection performance achieved by different methods on the nuScenes *val* set.

4. Experiments

4.1. Experimental Setup

We evaluate the effectiveness of our proposed model by conducting three downstream tasks on four autonomous driving datasets [25, 13, 30, 1]. To implement 3D object detection and unsupervised domain adaptation tasks, we utilize the popular point clouds detection codebase Open-PCDet [31] (version 0.5.2). For 3D semantic segmentation task, we use the open-sourced Cylinder3D [46] as the pre-trained backbone, which applies the cylindrical voxel partition. We first pre-train the Occupancy-MAE on the unlabeled raw set of the ONCE dataset and then fine-tune the perception model on the training set. However, for the KITTI, Waymo, and nuScenes datasets, pre-training and fine-tuning are both on the training set. The ONCE dataset provides a benchmark for self-supervised learning methods, but no codes are available. Thus, we only compare our Occupancy-MAE with self-supervised learning methods on the ONCE dataset.

In our experiments, we set the masking ratio for voxels within 0-30 meters, 30-50 meters, and > 50 meters to 90%, 70%, and 50%, respectively. The number of pre-training epochs is 3. For more detailed parameter setups, please refer to OpenPCDet [31, 25] and Cylinder3D [46].

4.2. Results on Downstream Tasks

4.2.1 3D Object Detection

We begin by comparing our proposed method with several state-of-the-art self-supervised learning methods on the ONCE dataset [25] *val* set. These include two contrastive learning methods (BYOL [16] and Depth-Contrast [44]), two clustering-based methods (DeepCluster [3] and SwAV [4]), and two masked small-scale point

clouds autoencoding methods (Point-MAE [26] and MaskPoint [23]). Table 1 shows that our method, with the SECOND [39] detector as the pre-trained backbone, outperforms the self-supervised methods in terms of mAP. Our method achieves a 2% ∼ 6% performance gain over contrastive learning methods because the contrastive views of a 3D scene by data augmentations may be similar, causing the model to converge to a trivial solution [25]. Our Occupancy-MAE achieves comparable results with SwAV [4] and DeepCluster [3], with marginal improvement, but it is much simpler than clustering-based methods. Masked small-scale point clouds autoencoding methods cannot be directly applied to large-scale LiDAR point clouds. We replace the Transformer network of Point-MAE and MaskPoint with a 3D sparse convolutional encoder and a 3D deconvolutional decoder. Occupancy-MAE achieves a 1.4% ∼ 2% performance gain over Point-MAE and Mask-Point. We attribute the performance gain of our method to the range-aware masking strategy and occupancy prediction task, which help to learn high-level semantic information for large-scale outdoor LiDAR point clouds.

We present the performance of Occupancy-MAE on KITTI test set in Table 2. Due to the limited submission times of 3 for KITTI policy, we only evaluate Occupancy-MAE with SECOND [39]. Our method significantly improves 3D object detection results on the moderate level of cyclist class, from 52.08% to 54.84%, and on car class, from 72.55% to 72.87%. For bird-view detection of cyclist class, our approach outperforms training from scratch by increasing mAP by 4.62% on moderate levels of cyclist class.

Pillar-based methods, such as PointPillars [22] and SST [11], are variants of voxel-based methods with high computational efficiency. Pillar-based methods process point clouds in vertical columns (pillars), which may contain points of the road. We only consider the points above

Method	Epoch	mIoU	barrier	bicycle	bus	car	construction	motorcycle	pedestrian	traffic-cone	trailer	truck	driveable	others	sidewalk	terrain	manmade	vegetation
Cylinder3D [46]	15	70.22	71.5	16.7	88.2	85.2	40.5	71.5	68.5	61.1	56.7	79.9	96.0	**70.9**	72.3	73.2	86.2	85.3
	25	70.83	72.5	17.1	88.2	**85.3**	**46.0**	71.3	73.7	58.7	**61.9**	**81.0**	96.0	66.0	71.9	71.6	86.6	85.4
Occupancy-MAE + Cylinder3D	15	71.61	72.6	29.3	**89.4**	84.3	40.4	77.7	73.4	60.1	58.2	77.0	96.0	69.9	72.2	**73.7**	86.3	**85.5**
	25	**72.85**	**74.6**	**33.0**	89.3	85.2	40.9	**78.6**	**75.9**	**62.9**	61.5	79.3	**96.1**	70.5	**72.7**	72.7	**87.2**	85.4

Table 6. Quantitative segmentation performance achieved by different methods on the nuScenes *val* set.

Task	Method	PV-RCNN BEV	3D
Waymo → KITTI	Oracle	88.98	82.50
	Source-only	61.18	22.01
	ST3D [40]	84.10	64.78
	Occupancy-MAE + ST3D	**85.52**	**65.24**
nuScenes → KITTI	Oracle	88.98	82.50
	Source-only	68.15	37.17
	ST3D [40]	78.36	70.85
	Occupancy-MAE + ST3D	**78.66**	**71.24**

Table 7. Quantitative results of unsupervised domain adaptation methods on the KITTI *val* set.

Figure 3. (a) Data efficiency of Occupancy-MAE. (b) Comparison of different masking strategies.

the road to build the occupancy labels. In Table 3, we show that Occupancy-MAE improves training from scratch by approximately $1\% \sim 2\%$ performance gains on the pedestrian and car classes. Additionally, Occupancy-MAE outperforms Voxel-MAE [20] by around $1\% \sim 1.5\%$ mAP, as the target of Occupancy-MAE (occupancy structure above the road) is more reasonable than regression of the points and pillar occupancy of Voxel-MAE [20].

We evaluate Occupancy-MAE on the Waymo *val* set and present the results in Table 4. Our pre-trained model outperforms training from scratch, especially for small objects, achieving approximately $1\% \sim 2\%$ performance gains on the pedestrian and cyclist classes. Small objects contain only a few points, making them challenging to detect. The masked occupancy reconstruction task enables the network to fill in missing occupancy information, thereby improving the detection of small objects.

Lastly, we verify the effectiveness of Occupancy-MAE on nuScenes dataset and report the results in Table 5. The performance improvement on nuScenes (32-beam) is limited because the point clouds are sparser than those in KITTI and Waymo (64-beam). Moreover, the high masking ratio of 90% is not suitable for very sparse point clouds. We report results for SECOND [39], CenterPoint [41], and PV-RCNN [27] from OpenPCDet [31] and ONCE [25].

4.2.2 3D Semantic Segmentation

For self-supervised learning on the 3D semantic segmentation task, We design the lightweight decoder of Occupancy-MAE with only two 3D Deconv layers. Table 6 shows
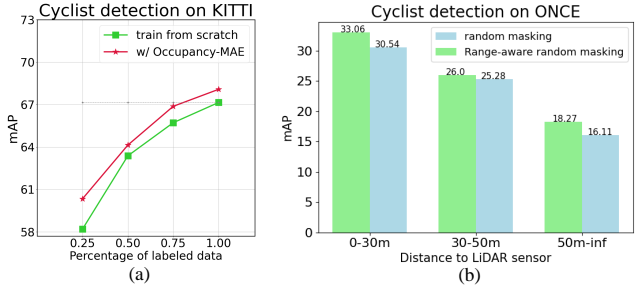
that Occupancy-MAE outperforms training from scratch by around 2% mIOU on nuScenes *val* set. This implies that Occupancy-MAE is well suited for 3D semantic segmentation task since our masked voxel classification objective promotes the model to capture the occupancy distribution of the 3D space, which is also very important for the dense prediction task, i.e. 3D semantic segmentation. Results in Table 6 were obtained by retraining Cylinder3D [46].

4.2.3 Unsupervised Domain Adaptation

The domain shifts in LiDAR-based 3D perception models are apparent as the LiDARs have different patterns. Evaluation of datasets captured in different locations or sensors results in a drop in model performance. To further investigate the generalization ability of Occupancy-MAE in representation learning, we conduct experiments in two scenarios of unsupervised domain adaptive (UDA) 3D object detection: different collection locations and time (i.e. Waymo → KITTI) and different LiDAR ring numbers (i.e. nuScenes → KITTI). We compare our method with Oracle, Source-only, and ST3D [40]. We follow the setting of the SOTA UDA method ST3D. We first train Occupancy-MAE on the source and target data simultaneously and then apply the pre-trained model to warm up the object detector in ST3D. Table 7 shows that pre-training with Occupancy-MAE further narrows the gap between UDA and Oracle by about $0.5\% \sim 1\%$ mAP. Our pre-trained network has a voxel-awareness of the object shape of the target data, which enables the UDA model to generate high-quality pseudo-labels for self-training.
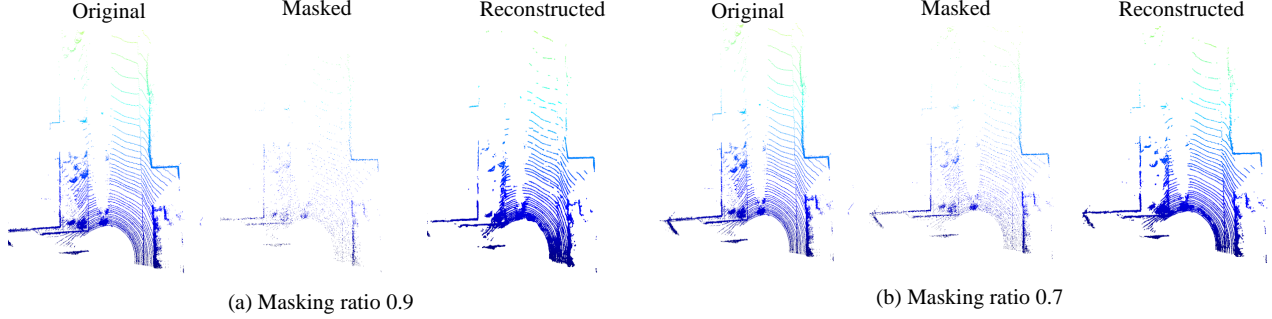
(a) Masking ratio 0.9   (b) Masking ratio 0.7

Figure 4. Masked occupancy reconstruction results of Occupancy-MAE with masking ratio 90% and 70% on KITTI dataset.

4.3. Ablation Studies

4.3.1 Data-efficient Learner

Pre-training enables fine-tuning of models using limited labeled data. To examine the data efficiency of Occupancy-MAE, we conducted experiments with varying amounts of labeled data used for fine-tuning, using SECOND [39] as the backbone, and evaluated its detection performance on the KITTI *val* set. Our results, shown in Figure 1 and Figure 3 (a), indicate that using Occupancy-MAE with 50%, 75%, and 75% of labeled data, respectively, results in the same performance as training from scratch with the full dataset for the car, pedestrian, and cyclist classes. With only 25% of the samples for fine-tuning, our Occupancy-MAE model improves performance by 1% ∼ 2% mAP over training from scratch, highlighting its data efficiency and ability to reduce the need for costly human-annotated 3D data.

4.3.2 Range-aware Random Masking

We study the effectiveness of the proposed range-aware random masking strategy. For range-aware random masking, the masking ratio for voxels within 0-30 meters, 30-50 meters, and > 50 meters is set to 90%, 70%, and 50%, respectively. We compare it with random masking (the masking ratio is set to 90% for all voxels). We can see from Figure 3 (b) that range-aware random masking surpasses random masking by 2.5%, 0.7%, and 2.1% mAP with ONCE raw set as the pre-training datasets. This demonstrates that the masking ratio for large-scale point clouds should be inversely proportional to the distance from the LiDAR sensor.

4.3.3 Occupancy prediction pretext task

The key to successful self-supervised learning is selecting a suitable pretext task. In this section, we evaluate the effectiveness of the occupancy prediction pretext task. We compare it with voxel feature regression loss, which replaces the binary occupancy classification loss. The results in Table 8 show that the performance of voxel regression task is similar to training from scratch. The classification task outper-

Target	Car	Pedestrian	Cyclist
PV-RCNN [27]	83.61	57.90	70.47
Features Regression	83.60	57.92	70.52
Occupancy Classification	**83.82**	**59.37**	**71.99**

Table 8. Comparison of different pretext tasks.

forms the regression task by 0.2%, 1.6%, and 1.4% of mAP on the car, pedestrian, and cyclist classes, respectively. We believe that occupancy prediction task is more challenging, and determining whether a voxel contains points is more important for 3D perception models. Using the simple occupancy classification task, the pre-trained network can become more aware of the object's shape, thereby enhancing the performance of downstream tasks.

4.3.4 Visualization

In Figure 4, we present a visualization of reconstructed occupancy voxels using masking ratios of 90% and 70%. The results demonstrate that Occupancy-MAE can effectively recover the masked voxels and produce satisfying reconstructed outputs. Even with a high masking ratio of 90%, Occupancy-MAE can still capture the overall structure of the 3D scene, indicating that it learns useful representations.

5. Conclusion

This paper introduces Occupancy-MAE, a self-supervised masked autoencoding framework for pre-training large-scale outdoor LiDAR point clouds that utilizes vast unlabeled data in autonomous driving. Occupancy-MAE predicts the masked occupancy structure of the entire 3D scene, forcing the network to learn features that accurately deduce masked points. We propose the range-aware random masking strategy to improve pre-training performance for distant objects. Experimental results demonstrate that Occupancy-MAE is effective in various downstream tasks, such as 3D object detection, semantic segmentation, and unsupervised domain adaptation.

References

[1] Holger Caesar, Varun Bankiti, Alex H Lang, Sourabh Vora, Venice Erin Liong, Qiang Xu, Anush Krishnan, Yu Pan, Giancarlo Baldan, and Oscar Beijbom. nuscenes: A multimodal dataset for autonomous driving. In *Proceedings of the IEEE/CVF conference on computer vision and pattern recognition*, pages 11621–11631, 2020. 1, 2, 6

[2] Fabio M Carlucci, Antonio D'Innocente, Silvia Bucci, Barbara Caputo, and Tatiana Tommasi. Domain generalization by solving jigsaw puzzles. In *Proceedings of the IEEE/CVF Conference on Computer Vision and Pattern Recognition*, pages 2229–2238, 2019. 4

[3] Mathilde Caron, Piotr Bojanowski, Armand Joulin, and Matthijs Douze. Deep clustering for unsupervised learning of visual features. In *Proceedings of the European conference on computer vision (ECCV)*, pages 132–149, 2018. 4, 5, 6

[4] Mathilde Caron, Ishan Misra, Julien Mairal, Priya Goyal, Piotr Bojanowski, and Armand Joulin. Unsupervised learning of visual features by contrasting cluster assignments. *Advances in Neural Information Processing Systems*, 33:9912–9924, 2020. 4, 5, 6

[5] Angel X Chang, Thomas Funkhouser, Leonidas Guibas, Pat Hanrahan, Qixing Huang, Zimo Li, Silvio Savarese, Manolis Savva, Shuran Song, Hao Su, et al. Shapenet: An information-rich 3d model repository. *arXiv preprint arXiv:1512.03012*, 2015. 2

[6] Xiaokang Chen, Mingyu Ding, Xiaodi Wang, Ying Xin, Shentong Mo, Yunhao Wang, Shumin Han, Ping Luo, Gang Zeng, and Jingdong Wang. Context autoencoder for self-supervised representation learning. *arXiv preprint arXiv:2202.03026*, 2022. 2

[7] Angela Dai, Angel X Chang, Manolis Savva, Maciej Halber, Thomas Funkhouser, and Matthias Nießner. Scannet: Richly-annotated 3d reconstructions of indoor scenes. In *Proceedings of the IEEE conference on computer vision and pattern recognition*, pages 5828–5839, 2017. 2

[8] (2022) Tesla AI Day. [online]. http://https://www.youtube.com/watch?v=jPCV4GKX9Dw. 3, 5

[9] Jacob Devlin, Ming-Wei Chang, Kenton Lee, and Kristina Toutanova. Bert: Pre-training of deep bidirectional transformers for language understanding. *arXiv preprint arXiv:1810.04805*, 2018. 2, 4, 5

[10] Carl Doersch, Abhinav Gupta, and Alexei A Efros. Unsupervised visual representation learning by context prediction. In *Proceedings of the IEEE international conference on computer vision*, pages 1422–1430, 2015. 4

[11] Lue Fan, Ziqi Pang, Tianyuan Zhang, Yu-Xiong Wang, Hang Zhao, Feng Wang, Naiyan Wang, and Zhaoxiang Zhang. Embracing single stride 3d object detector with sparse transformer. In *Proceedings of the IEEE/CVF Conference on Computer Vision and Pattern Recognition*, pages 8458–8468, 2022. 3, 6

[12] Hao Fu, Hanzhang Xue, and Ruike Ren. Fast implementation of 3d occupancy grid for autonomous driving. In *2020 12th International Conference on Intelligent Human-Machine Systems and Cybernetics (IHMSC)*, volume 2, pages 217–220. IEEE, 2020. 3

[13] Andreas Geiger, Philip Lenz, and Raquel Urtasun. Are we ready for autonomous driving? the kitti vision benchmark suite. In *2012 IEEE conference on computer vision and pattern recognition*, pages 3354–3361. IEEE, 2012. 1, 2, 6

[14] Spyros Gidaris, Praveer Singh, and Nikos Komodakis. Unsupervised representation learning by predicting image rotations. *arXiv preprint arXiv:1803.07728*, 2018. 4

[15] Benjamin Graham, Martin Engelcke, and Laurens Van Der Maaten. 3d semantic segmentation with submanifold sparse convolutional networks. In *Proceedings of the IEEE conference on computer vision and pattern recognition*, pages 9224–9232, 2018. 5

[16] Jean-Bastien Grill, Florian Strub, Florent Altché, Corentin Tallec, Pierre Richemond, Elena Buchatskaya, Carl Doersch, Bernardo Avila Pires, Zhaohan Guo, Mohammad Gheshlaghi Azar, et al. Bootstrap your own latent-a new approach to self-supervised learning. *Advances in neural information processing systems*, 33:21271–21284, 2020. 4, 5, 6

[17] Chenhang He, Ruihuang Li, Shuai Li, and Lei Zhang. Voxel set transformer: A set-to-set approach to 3d object detection from point clouds. In *Proceedings of the IEEE/CVF Conference on Computer Vision and Pattern Recognition*, pages 8417–8427, 2022. 3

[18] Kaiming He, Xinlei Chen, Saining Xie, Yanghao Li, Piotr Dollár, and Ross Girshick. Masked autoencoders are scalable vision learners. In *Proceedings of the IEEE/CVF Conference on Computer Vision and Pattern Recognition*, pages 16000–16009, 2022. 2, 4, 5

[19] Kaiming He, Haoqi Fan, Yuxin Wu, Saining Xie, and Ross Girshick. Momentum contrast for unsupervised visual representation learning. In *Proceedings of the IEEE/CVF conference on computer vision and pattern recognition*, pages 9729–9738, 2020. 4

[20] Georg Hess, Johan Jaxing, Elias Svensson, David Hagerman, Christoffer Petersson, and Lennart Svensson. Masked autoencoder for self-supervised pre-training on lidar point clouds. In *Proceedings of the IEEE/CVF Winter Conference on Applications of Computer Vision*, pages 350–359, 2023. 3, 4, 5, 7

[21] Stefan Hoermann, Martin Bach, and Klaus Dietmayer. Dynamic occupancy grid prediction for urban autonomous driving: A deep learning approach with fully automatic labeling. In *2018 IEEE International Conference on Robotics and Automation (ICRA)*, pages 2056–2063. IEEE, 2018. 3

[22] Alex H Lang, Sourabh Vora, Holger Caesar, Lubing Zhou, Jiong Yang, and Oscar Beijbom. Pointpillars: Fast encoders for object detection from point clouds. In *Proceedings of the IEEE/CVF conference on computer vision and pattern recognition*, pages 12697–12705, 2019. 5, 6

[23] Haotian Liu, Mu Cai, and Yong Jae Lee. Masked discrimination for self-supervised learning on point clouds. *arXiv preprint arXiv:2203.11183*, 2022. 2, 3, 4, 5, 6

[24] Reza Mahjourian, Jinkyu Kim, Yuning Chai, Mingxing Tan, Ben Sapp, and Dragomir Anguelov. Occupancy flow fields for motion forecasting in autonomous driving. *IEEE Robotics and Automation Letters*, 7(2):5639–5646, 2022. 3

[25] Jiageng Mao, Minzhe Niu, Chenhan Jiang, Hanxue Liang, Jingheng Chen, Xiaodan Liang, Yamin Li, Chaoqiang Ye, Wei Zhang, Zhenguo Li, et al. One million scenes for autonomous driving: Once dataset. *arXiv preprint arXiv:2106.11037*, 2021. 1, 2, 6, 7

[26] Yatian Pang, Wenxiao Wang, Francis EH Tay, Wei Liu, Yonghong Tian, and Li Yuan. Masked autoencoders for point cloud self-supervised learning. *arXiv preprint arXiv:2203.06604*, 2022. 2, 3, 4, 5, 6

[27] Shaoshuai Shi, Chaoxu Guo, Li Jiang, Zhe Wang, Jianping Shi, Xiaogang Wang, and Hongsheng Li. Pv-rcnn: Point-voxel feature set abstraction for 3d object detection. In *Proceedings of the IEEE/CVF Conference on Computer Vision and Pattern Recognition*, pages 10529–10538, 2020. 3, 5, 6, 7, 8

[28] Shaoshuai Shi, Li Jiang, Jiajun Deng, Zhe Wang, Chaoxu Guo, Jianping Shi, Xiaogang Wang, and Hongsheng Li. Pv-rcnn++: Point-voxel feature set abstraction with local vector representation for 3d object detection. *arXiv preprint arXiv:2102.00463*, 2021. 3, 6

[29] Shaoshuai Shi, Xiaogang Wang, and Hongsheng Li. Pointr-cnn: 3d object proposal generation and detection from point cloud. In *Proceedings of the IEEE/CVF conference on computer vision and pattern recognition*, pages 770–779, 2019. 4

[30] Pei Sun, Henrik Kretzschmar, Xerxes Dotiwalla, Aurelien Chouard, Vijaysai Patnaik, Paul Tsui, James Guo, Yin Zhou, Yuning Chai, Benjamin Caine, et al. Scalability in perception for autonomous driving: Waymo open dataset. In *Proceedings of the IEEE/CVF conference on computer vision and pattern recognition*, pages 2446–2454, 2020. 1, 2, 6

[31] OpenPCDet Development Team. Openpcdet: An open-source toolbox for 3d object detection from point clouds. https://github.com/open-mmlab/OpenPCDet, 2020. 6, 7

[32] Zhan Tong, Yibing Song, Jue Wang, and Limin Wang. Videomae: Masked autoencoders are data-efficient learners for self-supervised video pre-training. *arXiv preprint arXiv:2203.12602*, 2022. 4

[33] Eva AM van Dis, Johan Bollen, Willem Zuidema, Robert van Rooij, and Claudi L Bockting. Chatgpt: five priorities for research. *Nature*, 614(7947):224–226, 2023. 2

[34] Liang Xiao, Jiaolong Xu, Dawei Zhao, Zhiyu Wang, Li Wang, Yiming Nie, and Bin Dai. Self-supervised domain adaptation with consistency training. In *2020 25th International Conference on Pattern Recognition (ICPR)*, pages 6874–6880. IEEE, 2021. 4

[35] Saining Xie, Jiatao Gu, Demi Guo, Charles R Qi, Leonidas Guibas, and Or Litany. Pointcontrast: Unsupervised pre-training for 3d point cloud understanding. In *European conference on computer vision*, pages 574–591. Springer, 2020. 2, 4

[36] Zhenda Xie, Zheng Zhang, Yue Cao, Yutong Lin, Jianmin Bao, Zhuliang Yao, Qi Dai, and Han Hu. Simmim: A simple framework for masked image modeling. In *Proceedings of the IEEE/CVF Conference on Computer Vision and Pattern Recognition*, pages 9653–9663, 2022. 2

[37] Chenfeng Xu, Bichen Wu, Zining Wang, Wei Zhan, Peter Vajda, Kurt Keutzer, and Masayoshi Tomizuka. Squeeze-segv3: Spatially-adaptive convolution for efficient point-cloud segmentation. In *Computer Vision–ECCV 2020: 16th European Conference, Glasgow, UK, August 23–28, 2020, Proceedings, Part XXVIII 16*, pages 1–19. Springer, 2020. 2

[38] Jiaolong Xu, Liang Xiao, and Antonio M López. Self-supervised domain adaptation for computer vision tasks. *IEEE Access*, 7:156694–156706, 2019. 4

[39] Yan Yan, Yuxing Mao, and Bo Li. Second: Sparsely embedded convolutional detection. *Sensors*, 18(10):3337, 2018. 2, 3, 4, 5, 6, 7, 8

[40] Jihan Yang, Shaoshuai Shi, Zhe Wang, Hongsheng Li, and Xiaojuan Qi. St3d: Self-training for unsupervised domain adaptation on 3d object detection. In *Proceedings of the IEEE/CVF Conference on Computer Vision and Pattern Recognition*, pages 10368–10378, 2021. 7

[41] Tianwei Yin, Xingyi Zhou, and Philipp Krahenbuhl. Center-based 3d object detection and tracking. In *Proceedings of the IEEE/CVF conference on computer vision and pattern recognition*, pages 11784–11793, 2021. 3, 5, 6, 7

[42] Xumin Yu, Lulu Tang, Yongming Rao, Tiejun Huang, Jie Zhou, and Jiwen Lu. Point-bert: Pre-training 3d point cloud transformers with masked point modeling. In *Proceedings of the IEEE/CVF Conference on Computer Vision and Pattern Recognition*, pages 19313–19322, 2022. 2, 3, 4, 5

[43] Renrui Zhang, Ziyu Guo, Peng Gao, Rongyao Fang, Bin Zhao, Dong Wang, Yu Qiao, and Hongsheng Li. Point-m2ae: multi-scale masked autoencoders for hierarchical point cloud pre-training. *arXiv preprint arXiv:2205.14401*, 2022. 2, 3, 4, 5

[44] Zaiwei Zhang, Rohit Girdhar, Armand Joulin, and Ishan Misra. Self-supervised pretraining of 3d features on any point-cloud. In *Proceedings of the IEEE/CVF International Conference on Computer Vision*, pages 10252–10263, 2021. 4, 5, 6

[45] Yin Zhou and Oncel Tuzel. Voxelnet: End-to-end learning for point cloud based 3d object detection. In *Proceedings of the IEEE conference on computer vision and pattern recognition*, pages 4490–4499, 2018. 5

[46] Xinge Zhu, Hui Zhou, Tai Wang, Fangzhou Hong, Yuexin Ma, Wei Li, Hongsheng Li, and Dahua Lin. Cylindrical and asymmetrical 3d convolution networks for lidar segmentation. In *Proceedings of the IEEE/CVF conference on computer vision and pattern recognition*, pages 9939–9948, 2021. 2, 4, 5, 6, 7